

Topology at the Deconfinement Transition Uncovered by Inverse Blocking in $SU(2)$ Pure Gauge Theory with Fixed Point Action*

M. Feurstein, E.-M. Ilgenfritz, [†]
M. Müller-Preussker and S. Thurner
Institut für Physik, Humboldt-Universität zu Berlin, Germany

December 2, 2024

Abstract

Renormalization group transformations discussed recently in deriving fixed point actions are used to design a smoothing method which should replace cooling. By Monte Carlo simulation with fixed point action near to the deconfinement transition the vacuum structure is analyzed on smoothed configurations applying this technique. The effect of suppressing dislocations on infrared physics is discussed by comparing string tension and topological susceptibility χ_{top} between unsmoothed and smoothed configurations. In the confinement phase, χ_{top} is consistent with the phenomenological value, and χ_{top} is measured across the deconfinement transition. We estimate the density of the instanton liquid and find it related to Abelian monopole currents. The density of spacelike monopole currents is a confinement order parameter. Instanton size and instanton-monopole correlation length are obtained. Prospects for cluster analysis of topological charge are pointed out.

1 Introduction

Improved or perfect actions for gauge fields and fermions have become a topic of central importance in lattice gauge theories very recently [1]. The main objective

*Supported by a Visitorship of M. F. and S. T. at the Graduiertenkolleg "Strukturuntersuchungen, Präzisionstests und Erweiterungen des Standardmodells der Elementarteilchenphysik"

[†]Supported by the Deutsche Forschungsgemeinschaft under grant Mu932/1-4

is to minimize finite lattice spacing corrections. One interesting approach to improvement was guided by the desire to construct a fixed point action [2, 3] with respect to real space renormalization group transformations.

More specifically, only gauge fields have been considered in these papers [2, 3] being subject to a block spin transformation of scale factor two. This transformation explicitly maps the links U of a fine lattice (with lattice step a) to blocked links V of the next coarser lattice (with lattice step $2a$). In the context of fixed point actions, as a new concept the procedure of inverse blocking appears in Refs. [2, 3], leading back to certain U 's from given V 's. This is an operation playing an essential role in the construction of the fixed point action itself. Contrary to blocking, this prescription cannot be explicitly written down and does not, as a rule, give back exactly those U 's one has started from constructing the V 's.¹ It is the guiding idea of the present work to exploit this non-identity for the elimination of short-range fluctuations from generic gauge field configurations on the fine lattice. This is similar but not identical to the use of inverse blocking in Ref. [3] as a tool to construct a smoothly interpolating gauge field on the next finer lattice for a Monte Carlo ensemble of quantum (not classical) configurations.

The procedure of inverse blocking consists of searching for a *constrained minimum* of the fixed point action with respect to the fine links U , where the constraints are represented by a certain blocking kernel $T(U, V)$ (multiplied with a Lagrange parameter κ) which depends on the U 's and the *prescribed* blocked links V .

The interpolation provided by the inverse blocking technique has been stressed as an alternative to cooling methods for measuring the topological charge. Let us recall for which purposes connected to the topological charge cooling was found useful in the past. There are plaquette based (field theoretic or naive) definitions [4, 5] of topological density. In order to use them for the analysis of *individual* lattice configurations it was found indispensable to smooth Monte Carlo lattice configurations. Cooling [6, 7] was then the only known method to do that.² On the other hand, geometrically defined evaluations of the topological charge like those of Lüscher [8, 9] and of Phillips and Stone [10] give always integers Q , but in order to obtain *reproducible* measurements some smoothing was also found to be necessary [11, 12]. This has been attributed to the extinction of dislocations. To replace cooling by a well-defined operation of interpolation is an important technical achievement of Refs. [2, 3]. The question has not been addressed there, however, to what extent the smooth interpolations are well-behaved enough that the naive definition of topological charge can be used instead of the (computationally more demanding) geometric charge definitions.

¹There is an important exception from this rule: classical multi-instanton solutions on the lattice are reproduced under blocking followed by inverse blocking.

²Later on improved operators of field theoretic kind have been defined which can be written in terms of cooled gauge fields [21].

At this place some comments on cooling [6, 7] might be in order. This technique is undoubtedly important for the construction of approximate classical solutions on the lattice with periodic or specific boundary conditions. Apart from this, the technique has been used for a decade in order to uncover topological structure by stripping off quantum fluctuations. The Vienna group has investigated the correlation of instantons with static quark and with monopoles using this technique [13]. It is this latter use of cooling that has been criticized by many authors. It consists of the *unconstrained* iterative minimization of the action, starting from equilibrium configurations generated with this action in a Monte Carlo simulation at a certain coupling β . This is a local procedure which first drives to the formation of locally almost classical configurations. In fact, however, with Wilson's action these configurations turn later on into configurations (dislocations) which locally violate the lattice equations of motion strongly, but are still carrying topological charge (measured by the usual operators of topological density) $Q = \pm 1$.³ Dislocations are lattice discretization artefacts, typically one lattice spacing in size, which possess topological charge but have no continuum counterpart.

Cooling can be extended from Wilson's to any action. Guiding principles for changing the action can be the scale invariance of the action, the stability of instantons with respect to this action and a sufficiently large action of dislocations. If dislocations violate a so-called entropic bound for good topological excitations, having an action $S < \frac{6}{11}S_I$ ($S_I = 2\pi^2$ (for $SU(2)$)), they spoil the scaling behavior of the topological susceptibility in the continuum limit. This happens, for instance, in the case of Wilson's action [12, 15].

For lattice studies of hadronic phenomenology the cooling method has been extensively used by the MIT group [16]. The problem is that after several tens of cooling steps control is lost to what extent the cooled configurations are still characteristic for the quantum (Monte Carlo) ensemble at a particular scale and/or temperature. In the worst case one is studying merely a model (for instance the random instanton model [17]) rather than QCD, instead of testing the model against the theory. One has to carefully control the step size and the number of cooling iterations, when structures have to be interpreted physically. Recently, there has been a series of attempts to invent intelligent ways of cooling [18] by a clever choice of the action, such that the cooling process becomes self-controlled and stabilizes structures of size above a certain threshold.

With the method of inverse blocking one attempts to avoid these problems. The parameters of the best action, the optimal blocking parameter and the Lagrange parameter κ were required [2, 3] to yield, as the result of inverse blocking of any typical lattice configurations on the coarse lattice, a configuration on the next finer lattice which saturates the following inequality

$$\min_U (S_{FP}(U) + \kappa T(U, V)) \geq S_{FP}(V). \quad (1)$$

³In general, the problem of dislocations is a problem not only of the action, but also of the method to define the topological charge of a given lattice configuration [14].

Once this action had been determined, a number of its good properties have been pointed out which include scaling properties and the usefulness in order to describe instantons and topological charge on the lattice.

In the first of the two related papers [2] its usefulness has been examined in conjunction with the prescription that topological charge measurements have to be performed only on inversely blocked (fine) configurations. Instantons were put by hand on the coarse lattice. Only instantons with $\rho > 0.8$ were found to possess a nonvanishing topological charge in this sense and to have a fixed point action $\approx 2\pi^2$ independent of ρ . This statement says that there are no dislocations belonging to this family of configurations, *i.e.* topological configurations with Phillips–Stone charge $Q_{PS} = 1$ and with an action below the entropic bound. After this observation, the fixed point action could be expected to be safe in the sense, that the topological susceptibility should scale, but only if the topological charge definition includes inverse blocking. The smallest instanton constructed on the lattice had a radius between the lattice spacing of the fine and the coarse lattice. In the second paper [3] a simplified fixed point action was successfully tested for scaling of the deconfinement temperature, of the torelon mass, of the string tension and of the topological susceptibility. It has been stressed there that the *interpolation by inverse blocking* was necessary to accomplish this good scaling property of the latter. We will later quantify this important reservation. This was evidence that the fixed point action together with the prescription for measuring the topological charge successfully suppress dislocations in the quantum ensemble. Then, for finite temperature, the behaviour of the topological susceptibility across the deconfinement transition could be determined with better confidence avoiding the ambiguities of the cooling method [19, 20].⁴

In the present investigation we want to explore the feasibility of inverse blocking as a method to replace cooling with respect to various aspects of long range structure of gauge field. We are going to use it as a technique of smoothing Monte Carlo configurations. From now the word smoothing is exclusively used in this sense, to distinguish it from cooling (with physics depending on the not–well–defined number of iterations). In distinction to Ref. [3] we prefer to generate Monte Carlo configurations on the *fine* lattice. Concerning topological charge, we go beyond the scope of Ref. [3] in that we can quantify the efficiency of suppressing dislocations, and we demonstrate the capability of the method to expose finer details of the distribution of topological charge. We show that this technique preserves (to a large extent quantitatively) other long distance physics (string tension, monopoles). Each one of the independent Monte Carlo configurations, U^{MC} , is blocked into one V . Then, starting from U^{MC} , constrained minimization leads to U^{smooth} which is a smooth reconstruction of U^{MC} conserving the long wave modes which have been stored in V . Independ-

⁴We remark that the drop of the topological susceptibility defined with improved lattice operators of the topological density [21] was found to be much more dramatic [22] than in Ref. [3].

dent of the number of iterations that the minimization needs in practice, this combined action of blocking and minimization (inverse blocking) is considered as one well-defined step which is not intended to be iterated.

We are going to use Lüscher's charge [8, 9] instead of Phillips–Stone's [10] and will compare this with the naive topological density [4, 5] (which becomes non-perturbatively renormalized). The reason for using these definitions for the Pontryagin density is that we are interested not only in the topological susceptibility, but we want to analyze the clustering properties of the topological density in generic Euclidean configurations dominating the functional integral. This includes the study of two-point correlators of the topological density with itself and correlators with monopole currents. The density [23] and anisotropy [24] of monopole currents are studied as usual in the maximally Abelian gauge [25, 26]. A more thorough study of clusters of topological charge will be reported in a separate publication [27].

The paper is organized as follows. In section 2 we give details on the fixed point action used in this analysis, on blocking and in particular on its inversion, which produces the smoothed configurations. In section 3 we present results on the string tension. For symmetric lattices this serves to calibrate the lattice step size $a(\beta)$ according to the fixed point action. The finite temperature string tension is computed in the confined phase from Polyakov line correlators. These results give evidence that the string tension is largely conserved by smoothing. Section 4 contains our results on the gross topological features of smoothed configurations across the phase transition. This concerns the suppression of the topological susceptibility (stronger than the decrease of topological activity which approximately represents the number of instantons plus antiinstantons), and a strong suppression of spatial Abelian monopole currents. The deconfinement signals are enhanced compared with non-smoothed Monte Carlo ensembles. In section 5 we present results on topological charge density–density correlations and on monopole–instanton correlations. We close with the visualization of clusters of topological charge together with their accompanying monopole currents for typical confining configurations and point out topics for further work in section 6.

2 Fixed Point Action and Smoothing

2.1 Action and Blocking

The simplified fixed point action [3] is parametrized in terms of only two types of Wilson loops, plaquettes $U_{C_1} = U_{x,\mu,\nu}$ (type C_1) and tilted 3-dimensional 6-link loops (type C_2) of the form

$$U_{C_2} = U_{x,\mu,\nu,\lambda} = U_{x,\mu} U_{x+\hat{\mu},\nu} U_{x+\hat{\mu}+\hat{\nu},\lambda} U_{x+\hat{\nu}+\hat{\lambda},\mu}^+ U_{x+\hat{\lambda},\nu}^+ U_{x,\lambda}^+. \quad (2)$$

It contains several powers of the corresponding linear action terms as follows

$$S_{FP}(U) = \sum_{type} \sum_i \sum_{C_i} \sum_{j=1}^4 w(i, j) \left(1 - \frac{1}{2} \text{tr } U_{C_i}\right)^j. \quad (3)$$

The parameter of this action have been optimized in Ref. [3] and are reproduced in Table 1.

$w(i, j)$	$j = 1$	$j = 2$	$j = 3$	$j = 4$
$i = 1$ (plaquettes)	.3333	.00402	.00674	.0152
$i = 2$ (6-link loops)	.08333	.0156	.0149	-.0035

Table 1: *Weight coefficients of the simplified fixed point action*

The notions of blocking and inverse blocking which have entered the construction of the fixed point action need some explanation. Fat links $V_{x,\mu}$ are defined for $x_\nu = odd$ for all $\nu = 1, 2, 3, 4$ only. These are the nodes of the blocked lattice.⁵ The blocking transformation expresses a fat link in terms of the product of the two links along the fat link plus a sum over rectangular six 4-link staples bypassing the fat link:⁶

$$\begin{aligned} \tilde{V}_{x,\mu} = & c_1^{block} U_{x,\mu} U_{x+\hat{\mu},\mu} \\ & + \sum_{\nu \neq \mu} c_2^{block} \left(U_{x,\nu} U_{x+\hat{\nu},\mu} U_{x+\hat{\nu}+\hat{\mu},\mu} U_{x+2\hat{\mu},\nu}^+ \right. \\ & \left. + U_{x-\hat{\nu},\nu}^+ U_{x-\hat{\nu},\mu} U_{x-\hat{\nu}+\hat{\mu},\mu} U_{x-\hat{\nu}+2\hat{\mu},\nu} \right). \end{aligned} \quad (4)$$

The actual fat link $V_{x,\mu}$ is then obtained by normalization to $SU(2)$:

$$V_{x,\mu} = \frac{\tilde{V}_{x,\mu}}{\sqrt{\det(\tilde{V}_{x,\mu})}}. \quad (5)$$

The recommended parameters are [28]

$$\begin{aligned} c_2^{block} &= 0.12 \\ c_1^{block} &= 1 - 6 c_2^{block}. \end{aligned} \quad (6)$$

⁵The blocked lattice can be defined as well shifted by one fine lattice step along one or more directions.

⁶Strictly speaking, the selection of paths between the nodes of the coarse lattice and the choice of the parameters could also be a matter of optimization.

2.2 Inverse Blocking and its Practical Implementation

Inverse blocking consists in searching the constrained minimum with respect to the fine links U of a full action

$$S_{full} = S_{FP}(U) + \kappa T(U, V), \quad (7)$$

including, besides of the fixed point action, the blocking kernel

$$T(U, V) = \sum_{fat\ links} \left(\max_{W \in SU(2)} \left(\text{tr} \left(W^+ \tilde{V} \right) \right) - \text{tr} \left(V^+ \tilde{V} \right) \right) \geq 0 \quad (8)$$

with κ as Lagrange parameter. For reasons of readability, we have dropped the labels x, μ carried by the fat links $V_{x, \mu}$ (describing the blocked configuration) and by the $\tilde{V}_{x, \mu}$ expressed through the fine links according to (4).

Before entering the actual investigations described below, we have tested, using fine lattice configurations U which were Monte Carlo generated at various β -values and then blocked to V , which value of κ has to be used in the full action (7) steering the inverse blocking. One should saturate the inequality (1) with the final smoothed configuration. We could not reach that goal with $\kappa = 12$ (recommended in Ref. [28]). Instead, we have found that a Lagrange parameter $\kappa = 5.15$ guarantees saturating the inequality (1) to an accuracy of one to three per cent, depending on β . Presumably this difference is due to our different point of view from the finer lattice (compared with Ref. [2, 3] and the minimization schedule used there). We will discuss these differences below. We plan to repeat the optimization of the fixed point action from our point of view with respect to all parameters of the simplified action (3). For the purposes of the present investigation, however we have accepted the parameters of the fixed point action as given in Ref. [3] and have used our optimal Lagrange parameter.

In a relaxation sweep through the links of the coarse lattice, the fine links which are along the fat links are updated first. Then, in a sweep through the plaquettes of the coarse lattice, the fine links emanating from the center of the coarse plaquette are updated. This exhausts the constrained links. Finally all other fine links are updated with respect to $S_{FP}(U)$ alone. They are not part of any of the blocking staples in (4), since they are at a distance $\sqrt{2}$ from a parallel fat link. The linear (in the links U) terms of the fixed point action S_{FP} are considered as a contribution to the linear part of the full action (7), S_{lin} . The second (also linear in U) term in $T(U, V)$ (eq. (8)) is also part of S_{lin} . The sum of the corresponding staples deriving from S_{lin} (with or without contributions from $T(U, V)$) is - when normalized to $SU(2)$ similar to (5) - a preliminary U^{offer} for this (constrained or unconstrained) link. The change is accepted provisionally if the sum of the fixed point action $S_{FP}(U)$ (including now the higher powers) and the linear part of $T(U, V)$ is decreased, otherwise it is rejected (we reset $U^{offer} = U^{old}$). The whole configuration of (new or old) links U^{offer} is finally accepted to replace the old one, U^{old} , if the full action

$$S_{FP}(U^{offer}) + \kappa T(U^{offer}, V) \leq S_{FP}(U^{old}) + \kappa T(U^{old}, V) \quad (9)$$

would decrease. Only for this final decision, the first (nonlinear) part of $T(U, V)$ is calculated once per sweep. The sweep should be repeated until the minimum of the full action is reached. In our optimization runs to find κ , we have (for all κ values) never observed the rejection of a sweep in the final acceptance check (9).

We want to point out some differences with the inverse blocking technique as used in Ref. [3]:

(i) We create Monte Carlo configurations on the fine lattice. We have to do blocking first, followed by inverse blocking back to the original lattice. Therefore we could always use the Monte Carlo configuration U^{MC} as a good starting configuration for the constrained minimization, while the long wave length modes of U^{MC} were stored in V .

(ii) We have no reason to neglect any part of the fixed point action since the configurations are not smooth at all in the first iterations of the minimization process.

(iii) The authors of Ref.[3] were forced to follow a particular minimization schedule [29], which included several cooling iterations before they switched to constrained minimization with respect to (7) with a certain, further truncated fixed point action. We have found it absolutely necessary to apply constrained minimization (with the full action) right from the beginning. Any modification, e.g. beginning with several pure cooling steps before the constrained algorithm is applied, would have been dangerous. The relaxing configuration would forget too fast about the features stored in V , such that the following constrained minimization practically cannot recover the configuration U^{smooth} , at least within ≈ 100 iterations.⁷

(iv) It is unnecessary to speed-up the method, because less than ten iterations are sufficient to reach the minimum of the full action which (with our optimal κ !) lies within one to three per cent from the action of the blocked configuration V

$$S_{FP}(U^{smooth}) + \kappa T(U^{smooth}, V) \simeq S_{FP}(V) \quad (10)$$

saturating the inequality (1).

A typical relaxation process is recorded in Fig. 1. The upper curve shows the full action $S_{FP}(U) + \kappa T(U, V)$ versus the number of iterations, and the two horizontal lines show the action of the original Monte Carlo generated configuration $S_{FP}(U^{MC})$ and the action of the blocked configuration $S_{FP}(V)$. Before the first iteration the functional $T(U, V)$ vanishes by construction, such that the fixed point action is equal to the full action. Typically, in the configuration U^{smooth} the full action is shared roughly equally between the fixed point action $S_{FP}(U^{smooth})$ and the functional $\kappa T(U, V)$. In order to see this, in Fig. 1

⁷More refined ensemble algorithms designed for complicated action landscapes (genetic and/or evolutionary ones) could be of use here. This remark applies also to the optimization program for the fixed point action.

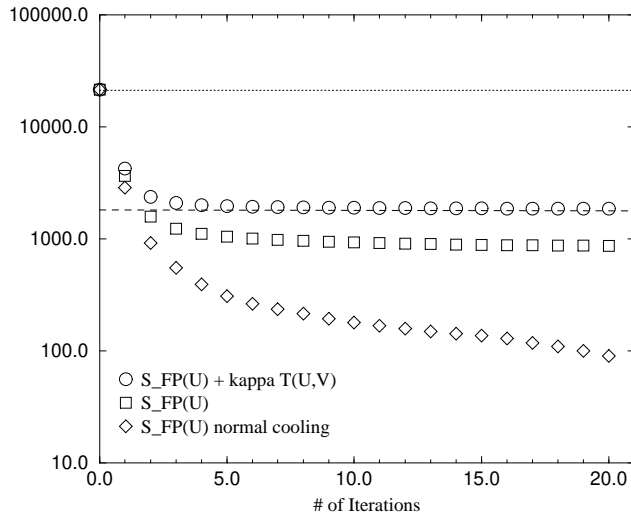


Figure 1: *Relaxation towards the smoothed configuration vs. cooling for a typical Monte Carlo configuration generated at $\beta = 1.5$ on a $12^3 \times 4$ lattice*

the history of S_{FP} alone is also shown by the middle curve. The history of S_{FP} beginning from the same starting configuration under cooling (i.e. when the constraint is dropped) is shown in the lower curve for comparison. Only two or three iterations of unconstrained minimization are sufficient to produce a configuration with a fixed point action less than one half of the action of the actual constrained minimum configuration.

3 Measuring the String Tension at $T = 0$ and at Finite Temperature

The inverse coupling constant β enters through the Gibbs weight

$$Z = \int DU \exp(-\beta S_{FP}(U)) \quad (11)$$

and defines the scale given by the lattice spacing $a(\beta)$ for the computation. Because we wanted to use the CPU intensive Lüscher charge, we have restricted ourselves to a lattice of size $12^3 \times 4$ for this finite temperature study. Measurements of the string tension at zero temperature for calibration purposes have been done on a 12^4 lattice.

For $L_t = 4$ the deconfinement transition is known to occur at $\beta_c = 1.575(10)$ [3]. This has been established by the crossing of the Binder cumulants of the Polyakov line for several spatial lattice sizes. We have not attempted to improve the localization of the deconfining transition or to do a finite size analysis. Rather than doing that, we have simulated at β -values safely lower ($\beta = 1.40$, $\beta = 1.50$ and $\beta = 1.54$) and higher ($\beta = 1.61$ and $\beta = 1.80$) than the deconfinement transition.

3.1 Calibrating the Lattice Using the Zero Temperature String Tension

Mainly in order to calibrate the lattice spacing a at each of the β -values to be used in the finite temperature simulations we have measured in a complementary simulation the zero temperature string tension on a 12^4 lattice. No topological analysis (with or without smoothing) has been attempted in this part of our calculations. We hope to come back to topological properties at $T = 0$ along the lines described in this paper in future work.

β	1.40	1.50	1.54	1.60	1.80
Monte Carlo	0.445(8)	0.245(3)	0.193(3)	0.124(2)	0.0380(9)
smoothed	0.228(4)	0.182(1)	0.156(3)	0.108(3)	0.0299(1)
Monte Carlo	152(3)	135(2)	129(2)	111(2)	91.7(19)
smoothed	77.9(10)	100.5(10)	104.5(20)	96.8(20)	71.2(20)

Table 2: String tension σa^2 (above) and σ/Λ_L^2 (below) at zero temperature from fuzzy Wilson loops in axial gauge on a 12^4 lattice (with two-loop expression for $a(\beta)\Lambda_L$)

The string tension has been obtained for Monte Carlo and smoothed configurations in the axial gauge from fuzzy Wilson loops. First, a certain direction has to be declared as Euclidean time. The axial gauge is enforced in chronological order time slice by time slice (except for the last one), putting each $U_4(x)$ to unity by applying a suitable gauge transformation $g(x + \hat{4})$ at the end of that link. Fuzzy Wilson loops are then calculated in this gauge. In fact, this is done by actively smearing the configurations. Smearing [30] is an iterative operation without change of scale which replaces each link U by U^{smear} through a procedure similar to (4) but with only one step in $\mu = 1, 2, 3$ direction and with only spatial one-plaquette staples involved ($\nu = 1, 2, 3$ $\nu \neq \mu$). In short, only spatial links are subject to spatial smearing. The timelike parts of the Wilson loops remain equal to unity (except for those beginning at the last time slice). This means that the fixed-time parts of the planar Wilson loops are replaced by a weighted sum over paths, running at fixed time and connecting the sites

of quark and antiquark. These sites are at a distance R in lattice units. The temporal extension of the Wilson loop is denoted as T . Motivated by the maximal spatial distance $R = 6$ of quark and antiquark, we have applied $N_{smear} = 6$ smearing iterations with an optimal smearing parameter (the notation is as in (4))

$$\begin{aligned} c_2^{smear} &= 0.125 \\ c_1^{smear} &= 1 - 4 c_2^{smear}. \end{aligned} \tag{12}$$

This parameter has been optimized in order to get a plateau of $\log(W(R, T + 1)/W(R, T))$ in T for the Monte Carlo configurations at $\beta = 1.5$. It has then been applied to all measurements, including those on smoothed configurations.

The potential is fitted (for all R) from exponential fits over the range $T = 2...5$. For the smoothed configurations we have restricted the fit range to $T = 3...5$. The potential $V(R)$ is then fitted with a 3-parameter fit that includes a constant, Coulomb and linear part over the range $R = 1...5$. For the smoothed configurations the Coulomb part is consistent with zero. The string tension from the linear part of the potential obtained for various β -values is presented in Table 2.

Although the string tension for smoothed configurations seems to have a scaling window (with respect to asymptotic scaling with the two-loop $a(\beta)$) ranging from $\beta = 1.5$ to $\beta = 1.6$ we will not extract the lattice spacings from these numbers. The string tension measured at $\beta = 1.8$ suffers from a small volume affect, since the spatial box size is at this β only $2.35/T_c$. Instead, we will use the data for Monte Carlo configurations in order to obtain a non-perturbative $a(\beta)$ with respect to an invariant string tension if this is conventionally measured (without smoothing).

The idea of blocking and inverse blocking suggests that the smoothed configurations U^{smooth} should faithfully represent the large scale physics shared by the original and the blocked configurations. Among those features the string tension is of primary importance, while the perturbative Coulomb part is not expected to survive smoothing. It should be reminded for comparison that the usual cooling of gauge field configurations conserves the string tension [31] as long as the topological susceptibility goes through a plateau (the cooling susceptibility is defined there [32]). The cooling used by the MIT group in order to measure hadronic correlation functions, for comparison, goes much too far to conserve the string tension [16].

The string tension in Table 2 largely confirms our expectation: 75 to 90 per cent of it (depending on β) remains after smoothing, with the exception of the lowest $\beta = 1.4$. For increasingly strong coupling the blocking and inverse blocking becomes less reliable to conserve the long range structure. This warning refers to the reproducibility with respect to a shift of the coarse lattice by one lattice unit of the fine lattice. Therefore we will exclude the lowest β -value from extracting a serious temperature dependence below.

3.2 Is the $T \neq 0$ String Tension Invariant under Smoothing?

Here we are going to discuss our results concerning the temperature dependent string tension $\sigma(T)$ and to clarify to what extent this quantity is insensitive to smoothing. Here we do the Monte Carlo generation of finite temperature configurations on asymmetric lattices of size $12^3 \times 4$. The string tension $\sigma(T)$ will have to vanish in the deconfinement phase at $\beta > \beta_c$. A suitable definition of the string tension for thermal lattices is provided by the correlator of Polyakov lines

$$L(\mathbf{x}) = \text{tr} \prod_{t=1}^{L_t} U_{\mathbf{x}t,4} \quad (13)$$

which, in the confinement phase, exhibits the confining potential in the form

$$\langle L(\mathbf{0})L(\mathbf{x}) \rangle \propto \exp(-V_{\bar{q}q}^{conf}(\mathbf{x})/T) \quad (14)$$

where $V_{\bar{q}q}^{conf}(\mathbf{x}) \sim \sigma(T)|\mathbf{x}|$ at large distances. At any distance, $V_{\bar{q}q}^{conf}(\mathbf{x})$ contains the self-energies of q and \bar{q} and the perturbative Coulomb potential, too. These are expected to be changed drastically under smoothing.

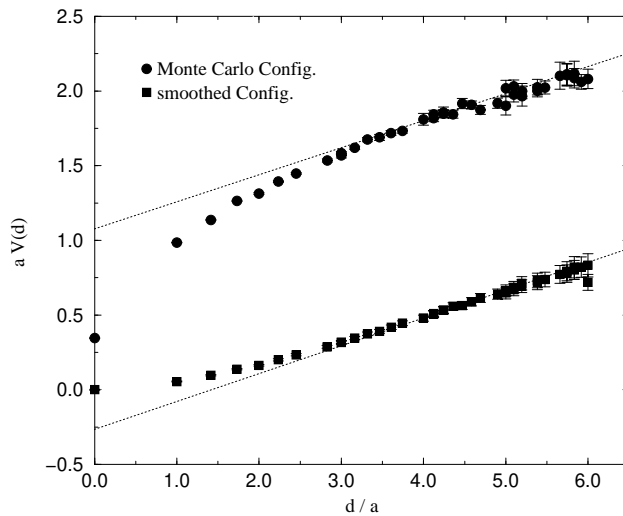


Figure 2: $\bar{q}q$ potential from Polyakov line correlators before (above) and after smoothing at $\beta = 1.5$ in the confinement phase

In the measurement of Polyakov lines and their correlators no smearing (cf. subsection 3.1 for the zero temperature string tension) is involved. The normalized correlators before and after smoothing can be directly compared

β	1.40	1.50	1.54
T/T_c	0.656	0.834	0.919
Monte Carlo	0.253(23)	0.193(4)	0.176(5)
smoothed	0.242(8)	0.189(2)	0.137(3)
Monte Carlo	86(8)	110(4)	118(4)
smoothed	83(3)	104(2)	92(2)

Table 3: *String tension $\sigma(T) a^2$ (above) and $\sigma(T)/\Lambda_L^2$ (below) from Polyakov line correlators at various temperatures $T < T_c$ in the confinement phase (with two-loop expression for $a(\beta)\Lambda_L$)*

for the three β -values in the confinement phase. Fig. 2 shows for $\beta = 1.5$ the logarithm of the (suitably normalized) Polyakov line correlator as function of the distance. In Table 3 we collect the extracted values of the string tension at the three temperatures in the confinement phase before and after smoothing. While there is an interesting temperature dependence, the string tension is really a long range effect that remains only moderately affected by the smoothing procedure. The reduction is less than 5 per cent at temperatures $T < 0.8 T_c$ and becomes more than 20 per cent at $T > 0.9 T_c$.

4 Gross Topological Features Near to the Deconfinement Transition

As a first result of our attempt to study topological structures of pure $SU(2)$ gauge theory near to the deconfining phase transition we obtain the behaviour of the topological susceptibility of pure $SU(2)$ gauge theory in this temperature range. Using inverse blocking as interpolation, this question has been studied already in Ref. [3] on lattices of invariable spatial size (both in lattice units L_s and physical units) by varying the temporal extent L_t . Contrary to that, we keep the lattice size $12^3 \times 4$ and vary β . Thus, this additional measurement might be interesting as well. Since we always block first and inversely block to the original lattice, there are also methodical differences pointed out in subsection 2.2 .

A complementary characteristics of confinement and the deconfining transition has been given in terms of the Abelian Dominance and the Dual Superconductor scenario through the activity of Abelian monopoles in certain gauges

[26]. We shall demonstrate how the elimination of short range fluctuations by means of the smoothing procedure sharpens this tool, too.

4.1 Measuring the Topological Susceptibility Across the Deconfining Phase Transition

We have measured for Monte Carlo configurations (separated by 20 updates) of the thermal lattice $12^3 \times 4$ the topological charge according to Lüscher's definition, $Q_{luescher}$ [8, 9], and using the naive topological density (defined in a spatially symmetrized way in terms of plaquettes [4])

$$q_{naive}(x) = -\frac{1}{2^9 \pi^2} \sum_{\mu, \nu, \sigma, \rho = -4}^{+4} \epsilon_{\mu\nu\sigma\rho} \text{tr}(U_{x,\mu,\nu} U_{x,\sigma,\rho}) \quad (15)$$

with

$$Q_{naive} = \sum_x q_{naive}(x) \quad (16)$$

(summed over lattice points) before and after the smoothing transformation described in the previous section. So far, the statistics amounts to 300 configurations for the unsmoothed measurements and 100 configurations for smoothed ones. There is no need to describe here details of the implementation of the Lüscher charge [9]. What is important for us is that it is also a sum of localized contributions

$$Q_{luescher} = \sum_x q_{luescher}(x) \quad (17)$$

(summed over hypercubes). The time consuming part of this algorithm is the numerical integration of a 2- and a 3-dimensional integral. Encouraging might be the observation that the evaluation of the topological charge on the smoothed configuration reduces the run time (function calls) by a factor of $\frac{1}{10}$ compared with that needed for the analysis of typical Monte Carlo configurations. The topological susceptibility is defined as

$$\chi_{top} = \frac{\langle Q^2 \rangle}{N_{sites} a^4}, \quad (18)$$

with charges Q corresponding in this paper to the naive and Lüscher's topological charge density. N_{sites} is the number of lattice points $L_s^3 \times L_t$ and the physical lattice volume is $N_{sites} a^4$. Data for Monte Carlo and smoothed configurations as function of T/T_c (without renormalization of the naive topological susceptibility) are collected in Table 4. We note that $\chi_{top}^{luescher}$ is changed under smoothing by one order (in the confinement phase) to two orders of magnitude (in the deconfinement). This means that the (simplified) fixed point action

χ_{top}	β	T/T_c	$\chi_{top}^{luescher}/\Lambda_L^4$	$\chi_{top}^{naive}/\Lambda_L^4$
Monte Carlo	1.40	0.656	0.224(17)10 ⁴	0.146(12)10 ²
	1.50	0.834	0.287(24)10 ⁴	0.370(27)10 ²
	1.54	0.919	0.310(27)10 ⁴	0.449(43)10 ²
	1.61	1.089	0.235(19)10 ⁴	0.753(59)10 ²
	1.80	1.732	0.190(16)10 ⁴	0.308(24)10 ³
smoothed	1.40	0.656	0.127(17)10 ³	0.84(11)10 ²
	1.50	0.834	0.358(47)10 ³	0.240(29)10 ³
	1.54	0.919	0.324(43)10 ³	0.239(30)10 ³
	1.61	1.089	0.138(25)10 ³	0.962(18)10 ²
	1.80	1.732	0.164(11)10 ²	0.100(70)10 ²

Table 4: *Topological susceptibilities in the Monte Carlo and smoothed samples (with two-loop expression for $a(\beta)\Lambda_L$)*

alone does not suppress topological excitations (of size a) in the quantum ensemble (in this β -range) which have to be smoothed away through blocking and inverse blocking. This corresponds to the finding in Refs. [2, 3] that a sensible measurement of topological charge needs inverse blocking, even in the case of geometrical definitions.

For usual Monte Carlo configurations (with Wilson action with a coupling in the range $\beta = 2.$ to 3.) the corresponding perturbatively calculated renormalization factor [33] is known to be small compared to one. (Furthermore, the lattice topological susceptibility contains additive terms due to mixing with other lattice operators including a perturbative tail.) Also with the fixed point action used in our Monte Carlo production of configurations, the apparent naive topological susceptibility in the confinement phase is not unexpectedly two orders of magnitude apart from the topological susceptibility defined through the integer valued and (not to be renormalized) Lüscher’s charge $Q_{luescher}$.

It is therefore very remarkable that after the smoothing transformation the susceptibilities χ_{top}^{naive} and $\chi_{top}^{luescher}$ differ by not more than 30 per cent. This remaining discrepancy is explained by Fig. 3 which shows a scatter plot of smoothed configurations in $Q_{luescher}$ and Q_{naive} which exhibits the very strong similarity of both charges. This leads to the definition of a renormalization factor of the naive charge $Z_q(\beta)$ for smoothed configurations

$$Z_q^{smooth} q_{cont}(x) a^4 = q_{naive}(x) a^4. \quad (19)$$

The corresponding numbers are collected in Table 5 for β -values below and above the phase transition.⁸ Recently a family of improved operators of topological

⁸For the highest β non-zero charges are very rare, such that the Z_q^{smooth} factor cannot be reliably measured in this way.

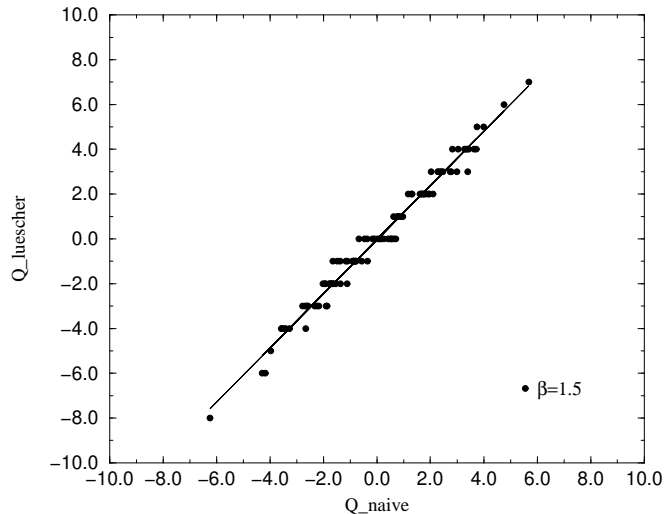


Figure 3: Scatter plot of Lüscher’s vs. naive topological charge for smoothed configurations at $\beta = 1.5$

β	1.50	1.54	1.61	1.8
$Z_q^{smooth}(\beta)$.826	.877	.843	–

Table 5: Effective renormalization Z_q factors of the naive topological charge density at various values of β on the $12^3 \times 4$ lattice

density [21] has been proposed. These operators are defined like in (15) but in terms of smeared links U^{smear} . This smearing - in contrast to our smearing in order to improve the Wilson loops - has to be applied to links in all directions and includes all six one-plaquette staples around the link to be smeared. The optimal smearing parameters are chosen in this case by minimizing the perturbative contribution to $Z_q^{smear}(\beta)$ which then is obtained nearly equal to one.

When the naive charge data in Table 4 are corrected with the squares of the $Z_q^{smooth}(\beta)$ factors from Table 5 we get a unique β -dependence of χ_{top} . We have shown in Fig. 4 this topological susceptibility for smoothed configurations. For the convenience of the reader, the lattice spacing $a(\beta)$ has been non-perturbatively expressed through the zero temperature string tension mea-

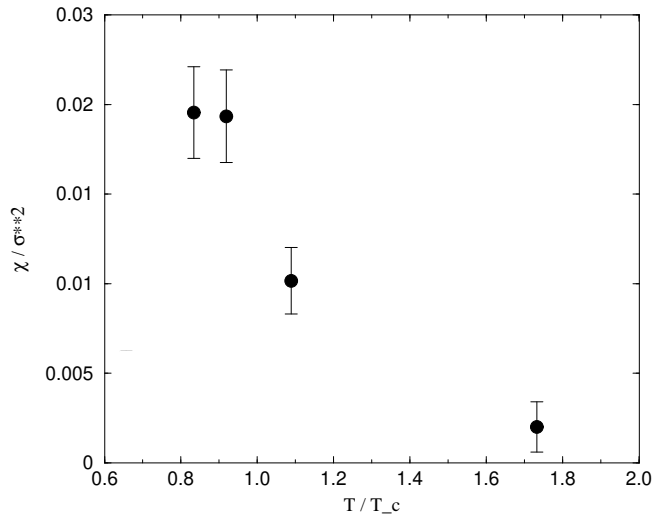


Figure 4: *Topological susceptibility for smoothed configurations across the deconfining phase transition for Lüscher’s topological density*

sured on the symmetric lattice at each corresponding β -value. We remind that for calibrating the lattice volume we have used the string tension as measured on the original Monte Carlo (not the smoothed !) configurations.

Assuming a string tension $\sigma = (440\text{MeV})^2$ we measure, for example at $T = 0.834 T_c$, a susceptibility $\chi_{top} = (165.5\text{MeV})^4$.

Instanton models use statistical mechanics to predict densities of instantons and antiinstantons and, eventually, correlations between them. QCD motivated assumptions on their interactions have to be made in these models. In order to verify or falsify these assumptions, one would like to extract at least the average density of instantons and antiinstantons from the lattice data besides of and independently from the topological susceptibility. If the configurations are predominantly represented by localized lumps of integer charge (this has been checked more thoroughly by a cluster analysis [27]) one could use, in addition to the total charge (eqs. (16) or (17)), the following operator to represent the number of instantons plus antiinstantons $N_+ + N_-$

$$A_{top} = \sum_x |q(x)|, \quad (20)$$

(for any definition of charge density). We can understand this, somewhat loosely, as a measure for the temperature dependent average glueball field (gluon conden-

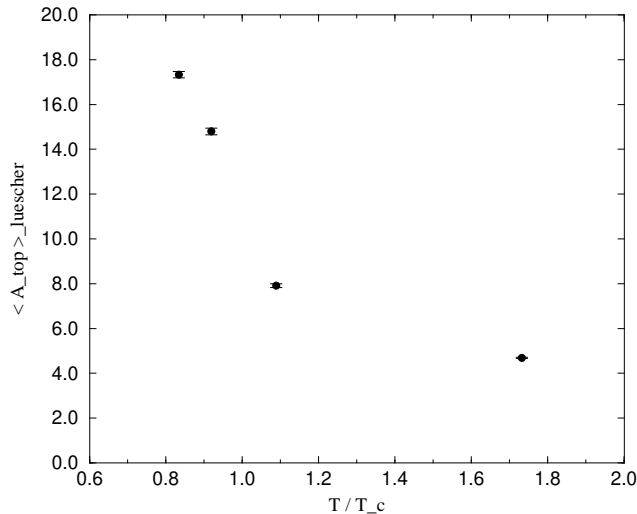


Figure 5: Average topological activity $\langle A_{top} \rangle$ (according to Lüscher's charge) of smoothed configurations as function of T/T_c

sate). In the following we call it topological activity. It is reduced by smoothing by a factor $\frac{1}{25}$ to $\frac{1}{40}$, depending on temperature. For unsmoothed configurations too much noise is contained in low values of $|q(x)|$ such that A_{top} is unreliable as an estimator of the number of instantons plus antiinstantons. In Fig. 5 we show the average topological activity of smoothed configurations as function of T/T_c . Between $\beta = 1.54$ and $\beta = 1.61$ ($T = 0.92 T_c$ to $T = 1.09 T_c$) it drops by a factor $\frac{1}{2}$, but the decrease becomes slower at higher temperature. For comparison, the topological activity measured on Monte Carlo configurations is less dramatically suppressed (by $\frac{1}{2}$ over the whole temperature interval).

Coming back to the smoothed configurations, the topological activity is only modestly suppressed, compared with the decrease of the topological susceptibility. Fig. 6 demonstrates mainly this additional suppression of *unpaired* topological charge in the deconfinement phase. Apart from this observation, an interesting low temperature bound is suggested (see the dotted horizontal line in Fig. 6) :

$$\chi_{top} \leq \frac{6}{11} \frac{\langle A_{top} \rangle}{N_{sites} a^4} = \frac{6}{11} \langle n_+ + n_- \rangle. \quad (21)$$

There is a factor $\frac{4}{b} = \frac{12}{11N_c}$ (equal to the entropic bound mentioned above) in this relation where b is the one-loop coefficient in the QCD β -function. A model

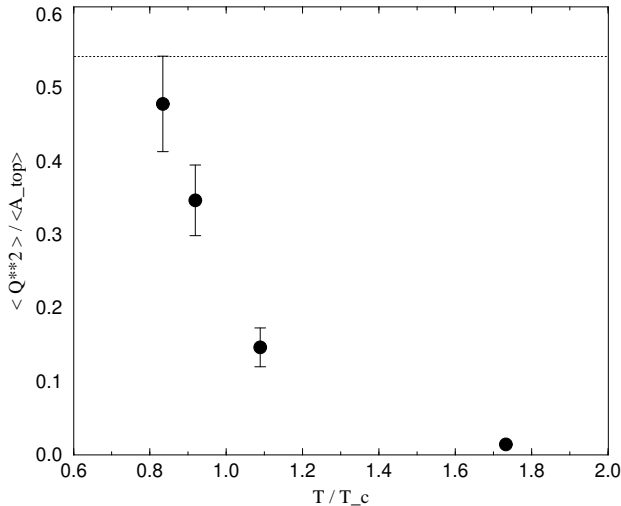


Figure 6: Ratio of topological susceptibility χ_{top} to average topological activity $\langle A_{top} \rangle / N_{sites} a^4$ (according to Lüscher's charge) of smoothed configurations as function of T/T_c

describing this $O(1/N_c)$ suppression of the topological susceptibility compared to the densities n_{\pm} of instantons and antiinstantons has been discussed by two of the authors in Ref. [34] in an instanton liquid model with scale invariant hard core interaction. A similar droplet model has been studied in Ref. [35].

Concluding this subsection, one can say that (i) the topological susceptibility is smaller by a factor $\frac{4}{b}$ than the topological activity at low temperature and that (ii) the topological susceptibility decreases more than the topological activity at the onset of deconfinement.

4.2 The Monopole Content of Smoothed vs. Monte Carlo Configurations

During the last ten years a complementary line of topological investigations has been pursued on the lattice relating the confinement property of Non-Abelian theories through the concept of Abelian dominance to the appearance of Abelian monopoles. These can be exposed by putting the lattice configurations into the maximally Abelian gauge [25]. There are only few investigations that shed light on how this picture gets modified at the deconfinement transition and in the deconfined phase [24]. Abelian dominance is expected to become manifest at

large distances. Therefore it is natural to study these aspects in the ensemble of smoothed configurations, too.

It is not necessary here to recall the prescription how to do the Abelian projection. Finally, configuration by configuration are mapped to corresponding Abelian ones where the links are represented by $U(1)$ phase factors. On this ensemble of configurations, confinement can be studied either in terms of the Abelianized link variables or, alternatively, in terms of the monopole currents. These can be detected by observing a net magnetic flux through the surface of a 3-dimensional cube. Each time a non-zero flux is detected, the dual (with respect to the cube) link x, μ is said to carry a monopole current $m_\mu(x)$. We

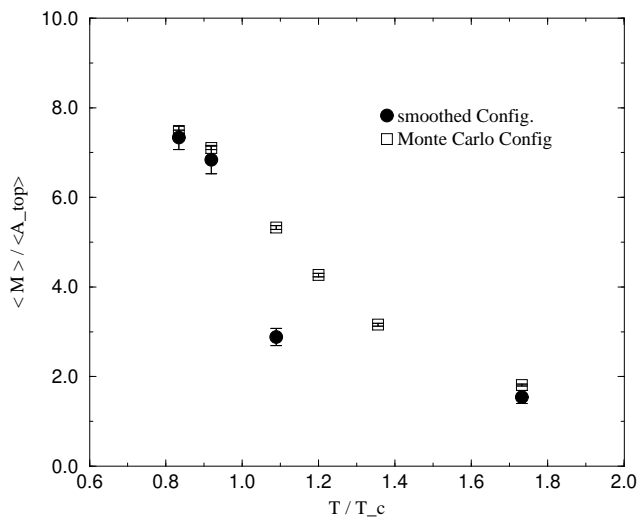


Figure 7: *Ratio between the averages of total monopole current number M and topological activity A_{top} as function of T/T_c for Monte Carlo and smoothed configurations*

do not enter here the issue of the correct description of monopole condensation [36] but restrict ourselves to measurements of the monopole current number

$$M_\mu = \sum_x |m_\mu(x)| \quad (22)$$

for spacelike ($\mu = 1, 2, 3$) and timelike ($\mu = 4$) dual links (and their sum M), the corresponding 3-dimensional densities and their respective temperature dependence.

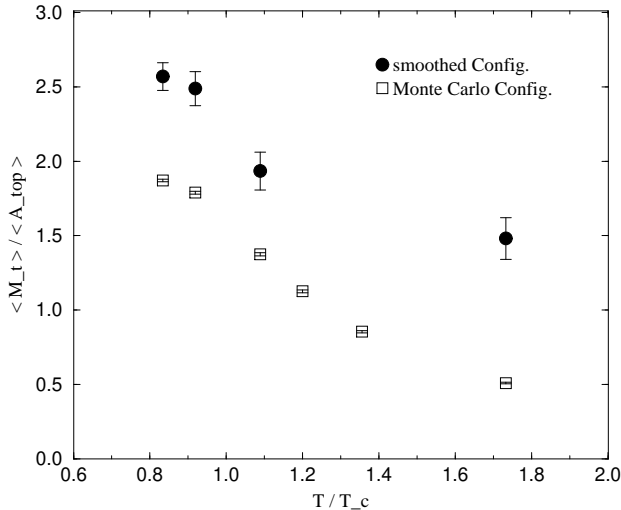


Figure 8: *Ratio between the averages of timelike monopole current number M_t and topological activity A_{top} as function of T/T_c for Monte Carlo and smoothed configurations*

There are indications that the monopole current number $M = \sum_{\mu} M_{\mu}$ is related to the topological activity A_{top} . Both quantities are reduced by the same factor $\frac{1}{25}$ to $\frac{1}{40}$, at the lowest and the highest temperatures, respectively, by the smoothing procedure. We show in Fig. 7 the ratio $\langle M \rangle / \langle A_{top} \rangle$. This ratio is smoothly falling with temperature across the phase transition for unsmoothed Monte Carlo configurations. For smoothed configurations, however, we find an order parameter like drop of this proportionality factor. This is mainly due to the spatially directed monopole currents. The corresponding ratio for timelike monopole currents alone (see Fig. 8) is a smooth function of temperature and changes on smoothed configurations between confinement and deconfinement even less.

The ratio between M_s (summed over $\mu = 1, 2, 3$) and $3 M_t$ ($\mu = 4$) is therefore expected to be an disorder parameter of confinement. This is obscured, however, by the much higher activity of monopole currents in the unsmoothed Monte Carlo configurations, but becomes very clear for smoothed configurations. For the original Monte Carlo configurations the monopole current number is almost space-time symmetric in the confinement phase and the ratio $\langle M_s \rangle / 3 \langle M_t \rangle$ changes only slightly over the β -range interpolating from the confinement to the deconfining phase. For the smoothed configurations, on the contrary, there is an

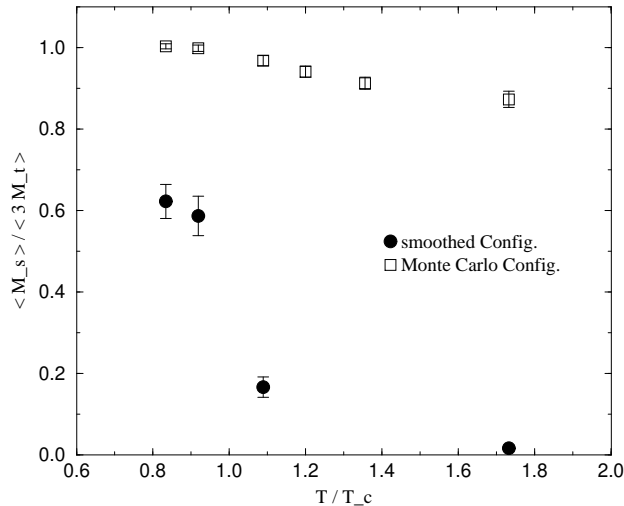


Figure 9: *Ratio between the averages of timelike and spacelike monopole currents across the deconfining phase transition for Monte Carlo and smoothed configurations*

surplus of timelike monopole currents already in the confinement phase (which probably can be interpreted as a finite L_t effect which is produced in the process of smoothing), but a complete extinction of spacelike monopole currents in the deconfined phase. In Fig. 9 the ratio $\langle M_s \rangle / 3 \langle M_t \rangle$ is compared for unsmoothed and smoothed configurations as function of β . Fig. 10 expresses the monopole currents in the form of 3-dimensional densities

$$n_\mu = \frac{1}{N_{sites} a^3} \langle M_\mu \rangle \quad (23)$$

(in physical units) of timelike and spacelike monopoles for smoothed configurations as a function of β . Monopoles, condensed in the confining phase, become static (massive) particle-like objects in the deconfined phase with a density that rises with temperature (cf. Ref. [24]). One may speculate about their relation to 't Hooft–Polyakov monopoles.

Spacelike monopoles currents (responsible for confinement below T_c) have completely disappeared at $T \simeq 1.7 T_c$.

5 Resolving the Vacuum Structure

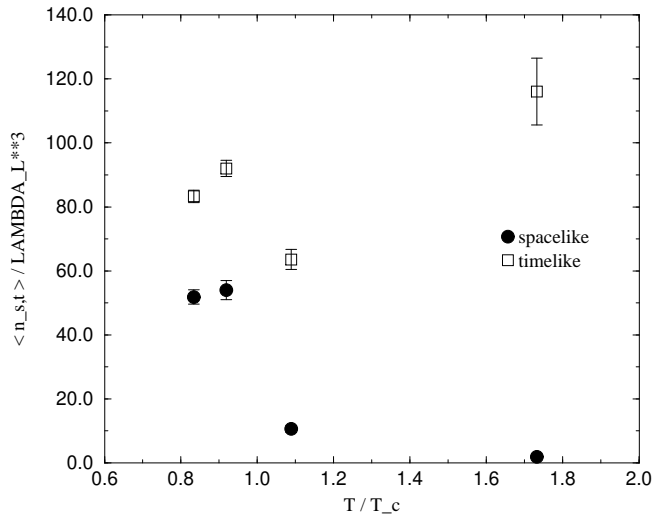


Figure 10: 3-dimensional densities of timelike and spacelike monopoles across the deconfining phase transition for smoothed configurations

5.1 Topological Density Correlation

Some information on the nature of topological excitations is contained in the point-to-point correlation function of the topological charge density. This is easy to measure, but for rough Monte Carlo configurations U^{MC} this measurement is of no value.

Several groups have attempted to define shape and size of topological excitations by the use of cooling techniques. The MIT group [16] has used for this purpose deeply cooled configurations. To this method the criticism expressed in the Introduction applies. Sometimes there appears a particular structure just during the first few cooling steps [13, 20]. The present method is welcome because it helps to detect structures in correlations measured on a set of well-defined configurations, being a smooth but local reconstruction of the corresponding rough Monte Carlo configurations.

In Fig. 11 we compare the normalized correlation function of the topological charge density measured on our $12^3 \times 4$ lattice in the confinement phase at $\beta = 1.5$ before and after smoothing. This figure describes the result of smoothing on the naive topological charge density correlator. Before smoothing, at any distance except for $x = 0$ there is practically no signal. In order to demonstrate the influence of temperature on the signal we show in this figure also the correlation function measured at $\beta = 1.8$ in the deconfinement phase. Due to the

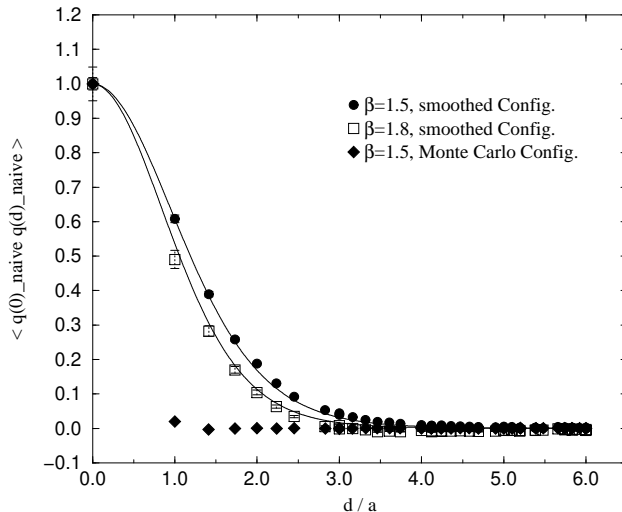


Figure 11: Normalized correlation function of the naive topological charge density at $\beta = 1.5$ (before and after smoothing) and at $\beta = 1.8$ (only smoothed)

normalization only the change of the instanton radius is described as explained below.

It is not due to an unfortunate choice of topological density definition (*i. e.* $q_{naive}(x)$) that smoothing is necessary in order to expose a signal in the density–density correlation function. This is demonstrated by Fig. 12 which shows the same for Lüscher’s charge density. The effect is similar, but the correlation of the naive charge density always extends somewhat farther which can be understood due to the extended nature of the operator (15).

By fitting the correlation function to the analytical shape derived from the instanton profile

$$q_{inst}(x) = \frac{6}{\pi^2 \rho^4} \left(\frac{\rho^2}{x^2 + \rho^2} \right)^4 \quad (24)$$

by folding

$$\langle q(x)q(0) \rangle \propto \sum_z q_{inst}(x-z)q_{inst}(z), \quad (25)$$

we have determined the average instanton radii ρ_{inst} as given in Table 6. The corresponding fitting curves are shown in Figs. 11 and 12. The instanton radius as determined by this method decreases more rapidly than the inverse

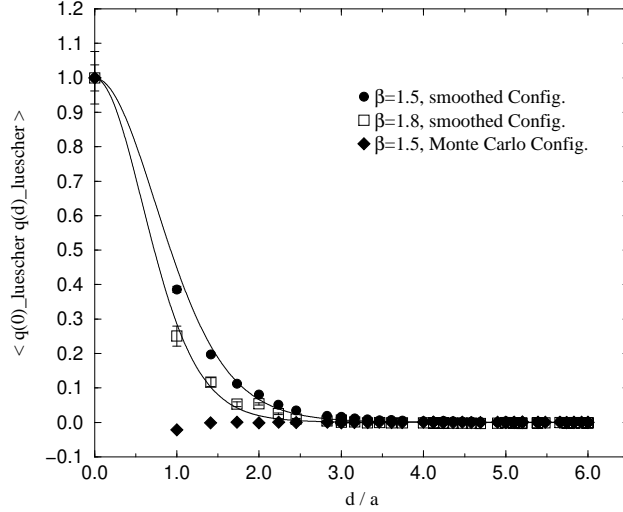


Figure 12: Normalized correlation function of the geometric Lüscher topological charge density at $\beta = 1.5$ (before and after smoothing) and at $\beta = 1.8$ (only smoothed)

temperature. Some change of ρ_{inst} at deconfinement has been observed by the cooling method, too [37].

β	1.50	1.54	1.61	1.80
Lüscher's charge	1.4 a	1.4 a	1.35 a	1.1 a
naive charge	1.8 a	1.8 a	1.75 a	1.6 a

Table 6: Instanton radii ρ_{inst} in lattice units as estimated from the topological charge density correlation function at two β -values in the confinement and two β -values in the deconfinement phase, according to the two charge definitions

Concerning the process of cooling (with Wilson action), on the contrary, it is known that the apparent average instanton radius as estimated by this type of correlation measurement grows slowly to $\rho_{inst} \approx 2.5 a$ after 25 and $\rho_{inst} \approx 2.8 a$ after 50 cooling steps starting from a Monte Carlo configuration in the confining phase [16].

5.2 Monopole–Instanton Correlation

It has been demonstrated before for certain classical configurations that there is a close connection between instantons and monopole world loops as becomes visualized in the maximally Abelian gauge [38]. A nontrivial correlation has

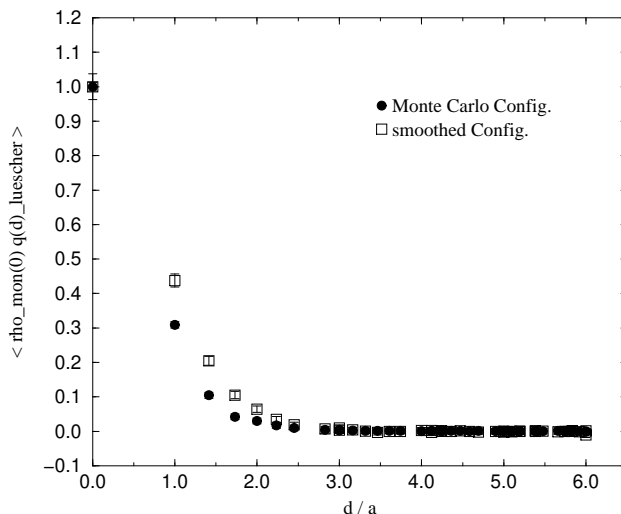


Figure 13: *Normalized correlation function of monopole currents with topological charge density (according to Lüscher) at $\beta = 1.5$ in the confinement phase*

been measured between topological charge density and monopole currents in the quantum state (Monte Carlo ensemble), too [13]. We show here in Fig. 13 the analogous correlator for the original Monte Carlo ensemble (generated with the fixed point action at $\beta = 1.5$ in the confinement phase) and the corresponding ensemble of smoothed configurations. The smoothed correlator is slightly wider, but there is no smoothing necessary to detect this correlation.

Comparing this with the same (normalized) correlation function at $\beta = 1.8$ in the deconfined phase, we find that they are identical as a function of the distance in lattice units within the error bars, *i. e.* the correlation length changes proportional to the inverse temperature.

6 Topological Clusters: Conclusion and Outlook

We have produced a set of (almost) classical configurations by cooling from hot starts using the simplified fixed point action (3). This set has then been

used for tests of our code of the smoothing algorithm. Our expectations for the technique have been fulfilled trivially by these particular lattice configurations. If one blocks a classical solution, one finds $S_{FP}(U) = S_{FP}(V)$. In Fig. 1 both horizontal lines would fall together. Inverse blocking reproduces then the original configuration since there is nothing to smooth. Not only the action is recovered but also the distribution of topological charge and the monopole currents. This is an important test that the smoothing method has to pass. But smoothing is intended to be applied to non-classical configurations.

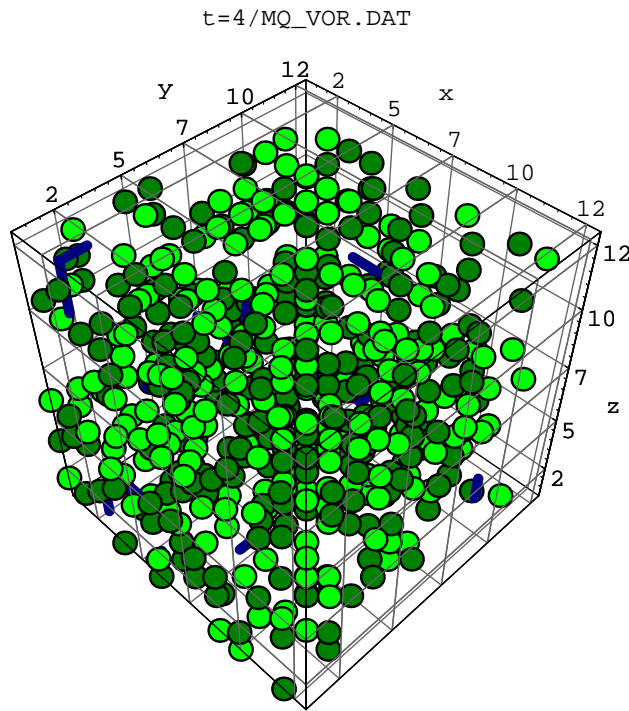


Figure 14: *Lüscher's topological charge density for $|q(x)| > q_0$ and monopole world lines in a timeslice of a typical Monte Carlo configuration in the confinement phase; signs of q are distinguished by different color*

We have explained in this paper how the smoothing procedure allows to analyze equilibrium configurations event by event and to lend support to possibly semiclassical scenarios of confinement (and of chiral symmetry breaking if the configurations would have been produced in non-quenched lattice QCD). Information on monopole currents was available without smoothing, too, but the number of monopole currents becomes smaller roughly proportional to the topological activity in the process of stripping-off quantum fluctuations. That

means that only a small part of them is really important for confinement because the string tension is largely unaffected. More than fitting the topological correlation function to some profile or to measure the monopole–instanton correlation function we are now in the position to investigate on the smoothed configurations clustering properties of the topological charge and to relate the clusters to the (now considerably more dilute) network of monopole currents. Instead of describing idealized semiclassical configurations this allows now to analyze vacuum lattice fields representative for the actual physical phase one is dealing with. The results might be interesting for model builders to check the reliability of their pictures of the vacuum. It would be interesting, too, how the lower part of the spectrum of the Dirac operator is influenced by smoothing.

One can easily study the spectrum of sizes, shapes and charges of clusters as well as their relative positions. Preliminary results [27] show that there are only clusters of topological charge ± 1 . The joint multiplicity distribution $P(N_+, N_-)$ of positive and negative clusters from simulations in the confinement phase and slightly above the deconfinement transition promises to be particularly interesting. The total cluster multiplicity distribution $P(N_+ + N_-)$ in the confinement phase is important for understanding low energy theorems in the framework of instanton models [39].

In Figs. 14 and 15 lattice hypercubes of one timeslice are depicted with a Lüscher topological charge density exceeding a threshold value. The original Monte Carlo configuration does not allow to guess any structure, whereas the smoothed configuration explicitly exposes it. There is no difference using either naive or Lüscher’s charge density. Therefore one can abandon to use the geometrical charges at all and to come back to the extremely cheap naive topological charge density.

A detailed analysis of the clustering properties of topological charge and the relation to the monopole currents in smoothed configurations is in progress [27]. It would be useful to repeat the analysis of the present work at higher $\beta \geq 1.8$ in order to avoid some of the finite L_t effects and in order to reduce the sensitivity with respect to the various coverings of the fine lattice by the blocked ones.

References

- [1] see F. Niedermayer, *e-print archive* hep-lat/9608097; W. Bietenholz, R. Brower, S. Chandrasekharan and U. J. Wiese, *e-print archive* hep-lat/9608068 (reports at LATTICE’96) and references therein
- [2] T. DeGrand, A. Hasenfratz and Decai Zhu, *e-print archive* hep-lat/9603015
- [3] T. DeGrand, A. Hasenfratz and Decai Zhu, *e-print archive* hep-lat/9604018

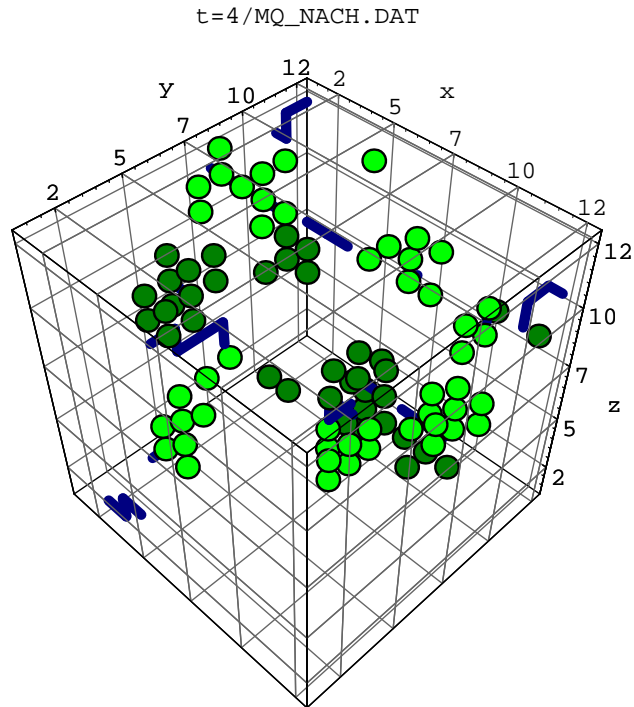


Figure 15: *Clustering of the Lüscher topological charge density and monopole world lines in a timeslice of the same configuration as in Fig. 14 but after smoothing*

- [4] P. Di Vecchia, K. Fabricius, G.C. Rossi and G. Veneziano, *Nucl. Phys. B* **192**, (1981) 392; *Phys. Lett. B* **108**, (1982) 323; *Phys. Lett. B* **249**, (1990) 490
- [5] N. V. Makhaldiani and M. Müller–Preussker, *JETF Pisma* **37**, (1983) 440
- [6] E.–M. Ilgenfritz, M. L. Laursen, M. Müller–Preussker, G. Schierholz and H. Schiller, *Nucl. Phys. B* **168**, (1986) 693
- [7] M. Teper, *Phys. Lett. B* **162**, (1985) 357
- [8] M. Lüscher, *Comm. Math. Phys.* **85**, (1982) 29
- [9] I. A. Fox, J. P. Gilchrist, M. L. Laursen and G. Schierholz, *Phys. Rev. Lett.* **54**, (1985) 749; A. S. Kronfeld, M. L. Laursen, G. Schierholz and U. J. Wiese, *Nucl. Phys. B* **292**, (1987) 330

- [10] A. Phillips and D. Stone, *Comm. Math. Phys.* **103**, (1986) 599; A. S. Kronfeld, M. L. Laursen, G. Schierholz, C. Schleiermacher, U. J. Wiese, *Comp. Phys. Comm.* **54**, (1989) 109
- [11] M. Müller–Preussker, in *Proc. XXVI Int. Conf on HEP*, Dallas 1992, J. R. Sanford (Ed.) (AIP 1993), Vol. II, 1545
- [12] D. J. R. Pugh and M. Teper, *Phys. Lett.* **B 218**, (1989) 326; **B 224**, (1989) 159
- [13] S. Thurner, M. Feurstein, H. Markum and W. Sakuler, *Phys. Rev.* **D 54**, (1996) 3457; S. Thurner, H. Markum and W. Sakuler, in *Proceedings of Confinement 95*, Osaka 1995, eds. H. Toki et al. (World Scientific, 1996) 77; H. Markum, W. Sakuler and S. Thurner, *Nucl. Phys.* **B** (Proc. Suppl.) **47**, (1996) 254
- [14] see, for instance, B. Berg and C. Panagiotakopoulos, *Nucl. Phys.* **B 251**, (1985) 353
- [15] M. Göckeler, A. S. Kronfeld, M. L. Laursen, G. Schierholz and U. J. Wiese, *Phys. Lett.* **B 233**, (1989) 192
- [16] M. C. Chu, J. M. Grandy, S. Huang and J. W. Negele, *Phys. Rev.* **D 49**, (1994) 6039; R. C. Brower, T. L. Ivanenko, J. W. Negele and K. N. Orginos, *e-print archive* hep-lat/9608086
- [17] T. Schafer and E. V. Shuryak, *Phys. Rev.* **D 53**, (1996) 6522; for a recent review, see T. Schafer and E. V. Shuryak, *e-print archive* hep-ph/9610451
- [18] M. Garcia Perez, A. Gonzalez–Arroyo, J. Snippe and P. van Baal, *Nucl. Phys.* **B413** (1994) 535; P. de Forcrand, M. Garcia Perez and I.–O. Stamatescu, *Nucl. Phys.* **B** (Proc. Suppl.) **47**, (1996) 278 and 777; *e-print archive* hep-lat/9608032
- [19] A. Di Giacomo, E. Meggiolaro, and H. Panagopoulos, *Phys. Lett.* **B 277**, (1992) 491
- [20] E.-M. Ilgenfritz, E. Meggiolaro and M. Müller-Preussker, *Nucl. Phys.* **B** (Proc. Suppl.) **42**, (1995) 496
- [21] C. Christou, A. Di Giacomo, H. Panagopoulos and E. Vicari, *Phys. Rev.* **D 53**, (1996) 2619
- [22] B. Alles, M. D’Elia, A. Di Giacomo, *e-print archive* hep-lat/9605013 and hep-lat/9607065
- [23] V. G. Bornyakov, E.–M. Ilgenfritz, M. L. Laursen, V. K. Mitrjushkin, M. Müller–Preussker and A. J. vander Sijs, *Phys. Lett.* **B 261** (1991) 116

- [24] V. G. Bornyakov, V. K. Mitrjushkin and M. Müller-Preussker, *Phys. Lett.* **B 284**, (1992) 99
- [25] A. S. Kronfeld, G. Schierholz and U. J. Wiese, *Nucl. Phys.* **B 293**, (1987) 461
- [26] A. S. Kronfeld, M. L. Laursen, G. Schierholz and U. J. Wiese, *Phys. Lett.* **B 198**, (1987) 516
- [27] M. Feurstein, E.-M. Ilgenfritz, S. Thurner and M. Müller-Preussker, *in preparation*
- [28] T. DeGrand, A. Hasenfratz, P. Hasenfratz and F. Niedermayer, *Nucl. Phys.* **B 454**, (1995) 587; *Nucl. Phys.* **B 454**, (1995) 615
- [29] A. Hasenfratz, *private communication*
- [30] M. Falcioni, M. Paciello, G. Parisi and B. Taglienti, *Nucl. Phys.* **B 251**, (1985) 624; M. Albanese et al., *Phys. Lett.* **B 192**, (1987) 163
- [31] M. Campostrini, A. Di Giacomo, M. Maggiore H. Panagopoulos and E. Vicari, *Phys. Lett.* **B 225**, (1989) 403
- [32] M. Campostrini, A. Di Giacomo and H. Panagopoulos, *Phys. Lett.* **B 212**, (1988) 206; M. Campostrini, A. Di Giacomo, H. Panagopoulos and E. Vicari, *Nucl. Phys.* **B 329**, (1990) 683
- [33] A. Di Giacomo and E. Vicari, *Phys. Lett.* **B 275**, (1992) 429; B. Alles, M. Campostrini, A. Di Giacomo, Y. Gunduc and E. Vicari, *Phys. Rev.* **D 48**, (1993) 2284
- [34] E.-M. Ilgenfritz and M. Müller-Preussker, *Phys. Lett.* **B 99**, (1981) 128
- [35] G. Münster, *Z. f. Phys.* **C 12**, (1982) 43
- [36] L. Del Debbio, A. Di Giacomo, G. Paffuti and P. Pieri, *Phys. Lett.* **B 355**, (1995) 255; M. N. Chernodub, M. I. Polikarpov and A. I. Veselov, *e-print archive* hep-lat/9512030 and hep-lat/9610007; M. I. Polikarpov, *e-print archive* hep-lat/9609020
- [37] M. C. Chu and S. Schramm, *Phys. Rev.* **D 51**, (1995) 4580
- [38] G. Schierholz and V. G. Bornyakov, *Phys. Lett.* **B 384**, (1996) 190; A. Hart and M. Teper, *Phys. Lett.* **B 371**, (1996) 261; M. N. Chernodub, F. V. Gubarev, *JETP Lett.* **62**, (1995) 100; R. C. Brower, K. N. Orginos and C.-I Tan, *e-print archive* hep-lat/9608012 and hep-th/9610101; M. Fukushima, S. Sasaki, H. Suganuma, A. Tanaka, H. Toki and D. Diakonov, *e-print archive* hep-lat/9608084 and hep-lat/9610003
- [39] D. I. Diakonov, M. V. Polyakov and C. Weiss, *Nucl. Phys.* **B 461**, (1996) 539